

Observations of nearshore wave dissipation over muddy sea beds

Sheremet A. and G. W. Stone

Coastal Studies Institute and Department of Oceanography and Coastal Sciences, Louisiana State University, Howe-Russell Geoscience Complex, Baton Rouge, LA 70803.

A. Sheremet, Coastal Studies Institute and Department of Oceanography and Coastal Sciences, Louisiana State University, Howe-Russell Geoscience Complex, Baton Rouge, LA 70803.
(ashere1@lsu.edu)

G. W. Stone, Coastal Studies Institute and Department of Oceanography and Coastal Sciences, Louisiana State University, Howe-Russell Geoscience Complex, Baton Rouge, LA 70803.
(gagreg@lsu.edu)

Abstract. Wave propagation on the Louisiana inner shelf is studied using concurrent measurements at two shallow water ocean observatory sites, in sedimentary environments dominated by mud at one site, and sand at the other. Contrary to the widely accepted hypothesis that mud-induced wave dissipation is important only for long waves, observations show significant damping of high frequency, short waves, which interact weakly with the bottom. The mechanism of short wave dissipation is not understood. Numerical simulations show that other dissipative processes such as refraction, or depth-limited breaking, do not account for the magnitude of the observed effects. Independent observations of strong sediment re-working during storms suggest that these effects are related to sediment resuspension processes.

1. Introduction

Studies of wave propagation in sandy environments commonly assume that the bathymetry is essentially unchanged over the characteristic wave evolution scales, with the exception perhaps of very energetic events. In contrast, cohesive sediments (fine silts and clays) are characterized by a fast response to flow forcing, resulting in a strong coupling between sediment and hydrodynamic processes. Gade's celebrated experiments [Gade, 1957], showing that 80% of wave energy can dissipate within a few wavelengths, underscore the efficiency of mud-induced wave attenuation, but also, implicitly, the strong response of the muddy bottom to wave motion. The collapse of two oil platforms in the Gulf of Mexico by Hurricane Camille in 1969, provides another extreme example. The platforms, designed to withstand hurricane-force winds and waves, were toppled by storm-induced mud fluidization [Sterling and Strohbeck, 1973].

Understanding the interaction between waves and muddy sea beds requires accounting for the evolution of mud rheology. The nonlinear character of mud dynamics, strongly dependent on strain state, has been established by field and laboratory measurements [Chou *et al.* 1993; Jiang and Mehta 1995]. Mud properties have been approximated using in turn poroelastic, viscoelastic, or viscoplastic (Bingham fluid) models [eg. Maa and Mehta 2000; Mei and Liu 1987]. A very helpful review of the classical work in wave-mud interaction can be found in Lee [1995]. A number of models for mud fluidization under waves and wave-mud interaction have been proposed, based on nonlinear, non-Newtonian rheological models [Foda *et al.*, 1993]. However, Mei and Liu [1987] note that, due to the great variety of fluid mud, and scarcity of field data, differing approaches may well have their own range of applicability.

Existing formulations of mud-induced wave dissipation are based on the assumption that the dominant mechanism is the interaction between waves and the soft sea bed. Such mechanisms can be efficient only if there is significant wave motion near the bottom, hence the “long wave paradigm”: dissipation effects are important only for long waves (low frequency waves, shallow water waves), which reach deep enough into the water column. Bottom sedimentary fabric should have negligible effect on short waves, which interact weakly with the bottom. The long wave paradigm has also influenced the planning of field experiments [Tubman and Suhayda 1976; Forristall and Reece 1985], with instruments typically deployed at two locations along the long wave propagation path, in deep and relatively shallow water (eg. 312 m and 20 m isobaths in Forristall and Reece 1985). Focusing on long wave propagation alone simplifies the problem by eliminating the need to account for wind input and wave breaking. Linear propagation models can be used to estimate refraction effects.

Ignoring mud effects on short waves is probably acceptable if the sea bed does not undergo significant re-working in the process. However, observations of sediment movement during storms on the Louisiana shelf [Allison et al., 2000], show that suspended fine-grained sediment can evolve significantly, from relatively low concentrations (0.1 g/l) and a horizontal stratification to almost constant concentration (1 g/l) throughout the water column. Short waves could be affected by sediment resuspension and deposition processes. Forristall and Reece [1985] and Wells and Kemp [1981] noted an increase in wave dissipation with wave energy, without investigating the source of this behaviour. Their work does not provide sufficient information regarding sediment characteristics to allow for correlating wave and sediment characteristics. Moreover, the typical pair of deep/shallow

water observation stations is not particularly suitable for studying short wave dynamics. The analysis and direct comparison of deep and shallow water short wave data can be difficult. With their evolution dominated by wind generation, nonlinearities and dissipation, short waves should lose phase coherency relatively quickly along the propagation path. In particular, one expects nonlinear coupling with long waves, and long wave dissipation, to intensify in shallow water, affecting strongly short wave transformation.

The objective of this work is to study mud-induced wave dissipation without imposing any *a priori* constraints on the frequency domain observed. To achieve this, an alternative experimental setting is used: rather than tracking wave transformation along propagation paths, we compare wave measurements taken at a muddy sea bed site to concurrent measurements from an “equivalent” sandy sea bed site. Here, the term “equivalent sites” is used meaning that wave measurements would be nearly identical at the sites, if sedimentary fabric of the sea beds were nearly identical. The two observation stations, one located south of Atchafalaya Bay (muddy environment), and the other south of Terrebonne Bay, (sandy environment), lie along the 5 m isobath, approximately 150 km apart, and are subject to similar wave generation and propagation conditions. Numerical models can be used, as in the past, to estimate refraction and linear shoaling effects. The fundamental assumption of “equivalence” of the locations is tested here using both measurements and numerical simulations.

Soft muddy sea beds are a notoriously difficult environment for instrument deployment, which explains, in part, the scarcity of available field data. Some of these difficulties have been overcome by the recent development, at Louisiana State University, of the WAV-CIS observation array (“Wave-Current-Surge Information System”, wavcis.csi.lsu.edu).

Despite constraints related to maintenance efforts, spatial coverage, and communication bandwidth, the array has provided a stable and comprehensive source of metocean field observations on the Louisiana inner shelf.

Section 2 provides details regarding the experimental setting, data acquisition and analysis techniques employed. Measurements are discussed in Section 3. Section 4 presents numerical simulation results. Conclusions and suggestions for future research are discussed in Section 5.

2. Experimental setting

The west Louisiana coast is the most active segment along the boundary between the fresh water system of the Mississippi River and the Gulf of Mexico, and is the subject of ongoing research [*Wells and Kemp* 1981; *Roberts et al.* 1989; *Allison et al.* 2000; *Walker and Hammack* 2000]. The region is under the influence of the Atchafalaya River, the largest tributary of the Mississippi River, which captures about 30% of its discharge, with an average suspended sediment load of 84 million metric tons per year (compiled by US Army Corps of Engineers, *Allison et al.* 2000). The large sediment influx from Atchafalaya Bay to the inner shelf carries almost half the volume of the Atchafalaya River [*Wells and Kemp*, 1981], and is responsible for mudflat accretion rates of up to 60-80 m/yr [*Roberts et al.*, 1989]. The mud plume, typically confined to shoreward of the 10 m isobath, has a highly variable structure which changes in response to atmospheric perturbations [*Walker and Hammack*, 2000]. Peak activity occurs in late winter and early spring months, coinciding with high Atchafalaya discharge levels and intense cold front activity [*Mossa and Roberts*, 1990]. Figure 1 illustrates the horizontal extent of surface

Figure 1

concentration of sediments using a Terra-1 Modis image taken after the passage of a cold front.

The observation site used in this study to monitor wave propagation in muddy environments is located near the 5 m isobath, approximately 20 km south of Marsh Island (station CSI 3 in Figure 1). The inner shelf adjacent to the station has a very low gradient, essentially flat at wave propagation scales (local slope is approximately 0.0002, with the 20 m isobath located some 50 km offshore). Away from scattered relict sandy shoals and reefs, bottom sediments are fine grained, with a mean particle diameter of 2-6 μm [Wells and Kemp, 1981]. Tides are low (mean amplitude 60 cm), with weak tidal currents [Wright *et al.*, 1997].

The recent development of WAVCIS has helped overcome technical challenges related to long term instrument deployment on the soft, muddy sea bed of the Atchafalaya shelf. Despite constraints related to maintenance efforts, spatial coverage, and communication bandwidth, which limit the scope of the observation data available, the WAVCIS program has provided the unprecedented opportunity to observe coastal processes under a wide range of atmospheric and sea conditions. WAVCIS is an array of observation stations distributed off the Louisiana coast, designed to operate in tropical cyclone conditions in the Gulf of Mexico. In 2002, the system withstood and operated successfully during four tropical cyclones, one of which (Lili) was a category 4 (Saffir-Simpson Scale) while in the central Gulf ([Stone *et al.*, 2003]). The project has five active stations, with three additional ones under construction, and monitors oceanographic (directional waves, currents, water level and temperature) and atmospheric (wind speed and direction, air temperature, barometric pressure, humidity and visibility) conditions. The stations use oil and gas

platforms for cabling and tethering instrumentation underwater, mounting atmospheric instrumentation on the upper decks and providing a power source for data post-processing on site. Data are telemetered onshore to Louisiana State University for quality control, archival, and dissemination.

One of the objectives of the WAVCIS project, monitoring of oceanographic processes in heterogeneous sedimentary environments, is reflected in the distribution of the observation stations along the Louisiana coast. Station CSI 5 (Figure 1) is located near the 5 m isobath, 3 km south of Timbalier Island, fronting Terrebonne Bay, off a sandy barrier coast where the transgressive sand sheet is being abandoned on the inner shelf [*Penland et al.*, 1988]. The distance between stations CSI 5 and CSI 3 is approximately 150 km. Atmospheric, tide, and offshore wave conditions are similar at the two sites. The shelf gradient is also low (local slope is 0.001, with the 20 m isobath approximately 25 km offshore). In contrast to the Atchafalaya shelf, the sedimentary composition at CSI 5 is dominated by quartzitic sands with a mean grain size of 0.1 mm [*Pepper and Stone*, 2002]. Station CSI 5 is used here as a source of concurrent wave data collected in a sand-dominated environment.

Collocated Paroscientific pressure sensors and Marsh McBirney current meters were installed at a depth of 2.5 m and 3.1 m at CSI 3 and CSI 5, respectively, as part of the WAVCIS array. Wave measurements consisted of hourly 16-min. time series of collocated pressure and current velocity, sampled at 4 Hz. The time series were processed using standard spectral analysis procedures (eg. *Earle et al.* 1995). Pressure and current meter data were quadratically detrended, and then divided into 64 s-long, demeaned sequences with 50% overlap. After tapering each sequence with a Hanning window, cross-spectra

and spectra with about 30 degrees of freedom and frequency resolution of 0.0156 Hz were calculated. The water depth at the sensors makes it difficult to estimate variance density values in frequency bands with $f > 0.3$ Hz, (where f is the frequency). To compensate for this effect, an f^{-4} spectral tail was used.

3. Observations

This study is based on wind and wave observations collected over 4 months, from January to April 2001. This period is part of the winter season, characterized by frequent cold front passages [*Mossa and Roberts* 1990; *Allison et al.* 2000; *Pepper and Stone* 2002]. Figure 2 illustrates some characteristic features of wind and wave observations associated with a typical storm, using time series of wind and wave parameters. For simplicity, the following discussion focuses on a single typical event, a cold front passing over the stations between January 28 and February 01, 2001 (grayed area in Figure 2).

Figure 2

The perturbation was typical of a winter season cold front passing over Louisiana. Pre-frontal winds out of the SE were relatively strong, with velocities of approximately 10 m/s, accompanied by significant wave heights of 1.5 m (variance approximately 0.15 m^2). As the front passed over the stations, wind direction veered to S, SW, and eventually to N. The approximate moment when the front passed over the stations is indicated by a sudden increase, then decrease in wind speed and a large scatter (uncertainty) of measurements of wind direction (afternoon of Jan. 29, Figure 2a,b). Post-frontal winds were weak, approximately 5 m/s. Although wind speed was slightly higher at CSI 3 compared to CSI 5, wind records are overall similar at the two stations, with no significant time lag, direction or magnitude difference. This suggests that the scale of the typical frontal perturbation is much larger than the distance between the two stations.

In contrast, wave measurements differ significantly, as shown in Figure 2c,d. While wave heights of about 1.5 m (0.15 m² variance) were recorded at CSI 5 at the peak of the storm, at CSI 3 waves exceeded 0.5 m (variance of about 0.015 m²) only very briefly (Figure 2c). The duration of relatively energetic waves was longer at CSI 5. Wave heights appeared to grow at similar rates at the two locations at the onset of the storm, however, post-frontal waves at CSI 3 decayed faster, and to lower values, when compared to CSI 5. CSI 5 was dominated by longer waves (mean period 5 s), with mean periods remaining roughly constant during the storm (Figure 2d); in contrast, mean periods at CSI 3 were about 1 s shorter initially and tended to approach CSI 5 values toward the end of the storm.

This behaviour is representative of the 4-month time series. Figure 3a compares variances measured at the two stations, for the entire data set. No data source closer to the shore than NDBC Buoy 42001 (about 450 km from CSI 3 and 350 km from CSI 5) was available for this study. For this discussion, data from the sandy site are used as reference. Variance measurements from CSI 5 rarely fall below 10⁻³ m², while CSI 3 variance stays below this value approximately 25% of the time. Almost the entire distribution lies between ratios 1 and 0.1, *i.e.*, for most of the time, waves are higher at CSI 5 than at CSI 3. The distribution also appears to have a non-trivial internal structure with data points clustering near ratios 1 and 0.1, depending on wave energy levels.

For low energy waves (e.g. CSI 5 variance < 10⁻²), wave variance at CSI 3 is between 0.2 to 0.3 of the value at CSI 5 for more than 75% of the record. As wave variance at CSI 5 increases, variance ratios show a tendency to group around both the 1 and 0.1 lines. The corresponding distribution of the mean periods, shown in Figure 3b, suggests

Figure 3

that the variance ratios of 1 and 0.1 may correspond to different sea states. Comparable variance levels (ratio 1) are associated with short waves; variance ratios close to 0.1 are associated with longer waves. The long wave paradigm provides a simple interpretation of these features. If long waves dominate offshore throughout the duration of the storm, they will also dominate at CSI 5 (sandy), but possibly not over the muddy sea bed at CSI 3, where they are attenuated by strong bottom friction. Short wave energy should be higher during the pre-frontal stage of the storm, when offshore SE winds are stronger. At CSI 3, the mean period shift suggests that short waves, which dominate at the onset of the storm, decrease in importance when wind forcing ceases.

The evolution of wave heights and mean periods exhibits a strong frequency dependence (eg. long versus short waves). Further information can be obtained by examining evolution trends of wave frequency spectrum at the two sites. For simplicity, the discussion will be limited to the event described above, the cold front passage, January 28 to February 01, 2001. The evolution of the frequency spectra is shown in Figure 4. Spectra computed for each 16-min. measurement burst are stacked in time to generate the surface plotted in Figures 4a,b, for stations CSI 5 and CSI 3 respectively. The associated wind speed and significant wave height time series are plotted for reference in Figure 4c,d). Since the following discussion focuses on frequency spectra, the terms “low/high frequency waves” are used in the sequel, rather than the equivalent “long/short waves”. The low and high frequency bands are defined here as $f \leq 0.2$ Hz and $f > 0.2$ Hz, respectively (dashed line in Figure 4a,b).

Figure 4

At CSI 5, Figure 4a, the energy distribution is dominated by a pronounced peak in the low frequency band, and exhibits a continuous increase and decrease during pre- and

post-frontal stages, with the peak attained at about the same time as the front passes over the station. At CSI 3, Figure 4b, low frequency waves evolve after a similar pattern, but at much lower energy levels. Evolution of higher frequencies bands is also significantly different at the two locations. At the beginning of the storm, high frequency waves appear to grow at similar rates at both sites. However, at CSI 3 they do not reach energy levels attained at the peak of the storm at CSI 5, and dissipate much faster behind the front, as the wind forcing weakens. As a result, the distribution at CSI 3 is assymmetrical on the time axis with respect to the storm peak.

The distinct behavior of the low and high frequency waves is illustrated in Figure 5, using time series of band-integrated variance, for the period covered in Figure 2. Figure 6 compares low and high frequency band variances for the entire observation period. Values of low frequency band variance (Figures 5a and 6a), differ by about one order of magnitude, regardless of sea state, but exhibit an almost perfect phase match. This is consistent with a friction-like wave-bottom interaction, which depends on the kinematics, rather than the dynamics, of wave propagation.

Figure 5**Figure 6**

The relationship between short wave energy at the two locations, Figures 5b and 6b, is more complicated, with energy ratios scattered over two orders of magnitude. For the entire data set, (Figure 6b), values cluster around the values of either 0.2 or 1. Figure 5b suggests a correlation with wind forcing, with high frequency waves responding rapidly to wind speed increase, reaching comparable energy levels, but falling off by about an order of magnitude during periods of calm weather at CSI 3. The distribution of wind speed, shown in Figure 7, supports this assumption. Variance ratios close to 1 are associated with wind speed values in the range of 10 m/s. Variance ratios closer to 10^{-1} are primarily

Figure 7

associated with calm weather (wind speeds of less than 4 m/s). This behavior is not consistent with wave breaking mechanisms, active for energetic waves (*i.e.* strong wind forcing). In addition, bottom friction should be weak at these frequencies: linear theory predicts that for periods smaller than 3 s, the variance of the wave motion is less than 5% of the surface value anywhere in the first 1 m above the seafloor.

The spatial distribution of surface concentration of sediment along the Louisiana Coast (Figure 1) suggests a correlation between sediment fabric and short wave dissipation. Recent observations have produced evidence of significant sediment re-working during winter storms, leading to sediment concentrations extending well beyond a near-bottom layer. Sediment resuspension could broaden the spectral range of wave-bottom interaction mechanisms. A substantial increase in suspended sediments appears to be typical of winter storms (*Walker and Hammack* 2000, Figures 4-5). Vertical sediment distributions can have complicated stratifications, with local maxima away from the bottom (*Murray et al.* 1997, Figures 121-122). Measurements by *Allison et al.* [2000] before and after a cold front passage (Figure 4 therein) show sediment concentration increasing during pre-frontal stages (from 0.1 g/l to 1 g/l) with isolines shifting from parallel to the bottom to bottom-normal (well mixed states). Remarkably, measurements taken near the 5 m isobath in the post-frontal stage (characterized by decreasing winds and sediment deposition), show the formation of what can be described as a fluid mud layer, with concentrations between 1 and 25 g/l. The mechanisms which govern the evolution of sediment concentration are not well understood. Estimates by *Walker and Hammack* [2000] indicate that 70-80% of the sediment load is resuspended locally by the wave field, the remainder being advected from Atchafalaya Bay. The hydrodynamics of cohesive sedimentary environments is a subject

of ongoing research. Equipment for long-term monitoring of sediment concentration is being deployed at all WAVCIS stations.

4. Numerical Simulations

An experimental setting based on equivalent stations located near the same isobath provides only a limited view of the spatial transformation waves undergo as they propagate across the shelf. However, information about spatial evolution is essential for assessing the importance of sediment induced dissipation effects relative to other processes, such as refractive scattering and depth-limited breaking. Unfortunately, deeper water, directional wave data were available for this study only from NDBC buoys. The position of the buoys closest to the experiment sites (buoys 42001, 42040, and 42019) are indicated by arrows in Figure 8. Buoy 42001 is located in the middle of the Gulf of Mexico, in deep water, some 400 km offshore. Buoys 42040, and 42019 are closer to the shore, to the east and west of the Louisiana coast, none directly fronting the study area. To correlate between wave data from the two sources (NDBS buoys on one hand and WAVCIS stations on the other), using numerical models, the computational grid had to be extended into deep water, increasing considerably the size of the domain (Figure 8 spans the entire computational grid used).

Figure 8

The size of the domain and large variations in water depth imposed severe constraints on the choice of numerical models, excluding, for example, time-domain Boussinesq models, and deep water spectral models. SWAN [*Booij et al.*, 1999], was the only numerical model available to us, which implements a level of wave physics detailed enough to simulate accurately wave propagation from deep to shallow water over scales of the order of 100 km. SWAN is a nonstationary, third generation nonlinear model, which accounts for, among other processes, refraction, shoaling, nonlinear four-wave interactions, bottom friction,

whitecapping, depth-limited breaking, and wave generation by wind. Robust advection schemes [Rogers *et al.*, 1999], also give SWAN the flexibility to describe wave propagation at a wide range of spatial scales and water depths. Some energy exchange mechanisms which are expected to be important over large scales in shallow water, such as near-resonant three-wave interactions, are poorly implemented in the model, and could not be accounted for in this study.

SWAN has no mechanism to account for the different sediment grain size or fabric, and as such, it cannot be used to simulate wave propagation processes specific to cohesive sedimentary environments. To the best of our knowledge, a model implementing correct mechanisms for mud-induced long wave dissipation was not available at the time of this study (given the growing interest in this problem, it will undoubtedly become available soon). The purpose of this study is not to derive or test such a model. It is important to stress that, for our purposes, such a model is also *not* necessary. Even without the correct dissipation mechanisms, SWAN can perform successfully two tasks essential to this study: the verification of the site-equivalence hypothesis on which the paper is based, and the assesement of the effect of other dissipation mechanisms. Numerical simulations presented here replace in effect the muddy bathymetry at CSI 3 by a sandy one of equal depth. They cannot be used to reconstruct directly wave evolution over the muddy sea bed at this site. They do, however, provide information regarding the strength of other dissipative mechanisms. Similar numerical results at the two observation sites would support the “equivalence” assumption, and point to the sedimentary fabric as the primary differentiating factor.

To achieve an acceptable resolution in the areas of interest, nested runs were performed with the wave model. SWAN was run first on a coarse grid at 4 km resolution. The extent of the grid represents a compromise between computational limits and the necessity of deriving meaningful boundary conditions from available data. The coarse grid runs were used to provide boundary conditions for the finer resolution grids (200 m grid step) in the neighbourhood of stations CSI 3 and CSI 5 (Figure 8). For the coarse grid, boundary conditions were interpolated from directional spectra measured at NDBC Buoys 42001, 42040, and 42019.

The sparsity of available wind data inside the modeling domain posed a serious problem, since wind fields associated with frontal passages are highly nonstationary and nonhomogeneous. Here, wind forcing was supplied by COAMPS [*Hodur, 1993*] 0 to 12-hr forecast (at 3-hr interval) of surface (10 m height) wind stations. Model winds tend to underestimate measured wind intensity at all stations shown, but the overall agreement between simulations and measurements is good. Figure 10, shows COAMPS surface wind distribution on Jan. 29, 2001, as the cold front passes over the stations. The perturbation is seen to extend beyond the deep water limit of the domain covered by the coarse grid. Because of the domain scale and the rather good representation of wind forcing, errors due to the misfit between wind direction near the boundaries and sparse wave boundary data are expected to have negligible effect inside the domain.

Figure 10

Wave propagation was simulated for the winter storm which affected the region between Jan. 27 and Feb. 01, 2001, discussed in Section 3. The front was rather well defined in the model winds by a sharp rotation in wind direction (Figure 10). SWAN was run in nonstationary mode, initialized with the stationary wave field computed for Jan. 27, a

day characterized by relatively low winds and waves. Starting the model with low initial waves allowed it to spin up forced by winds and boundary conditions alone, and helped reduce the effects of inaccuracies in initial conditions.

Figure 11a,b summarizes the spectral evolution of simulated wave fields at the two sites, in the same format as Figure 4. Figure 11c,d plots surface winds (COAMPS) and the significant height of simulated waves. Frequency spectrum evolution and time series of wind and wave height are smoother in these plots due in part to the coarser time resolution (3 hr, imposed by surface winds, 1 hr in Figure 4). Numerical results can be compared directly with the observations for the sandy environment at CSI 5, since SWAN implements parameterizations of wave-bottom interaction characteristic for the sandy environment (Figures 4a and 11a). The simulations underestimate the energy in the sea band and the mean swell period, but capture the general evolution trend fairly well, given the inaccuracies due to poor boundary data resolution and the use of numerical wind fields.

Figure 11

As discussed above, numerical results for CSI 3 cannot be compared directly to measurements. However, since SWAN represents the environment at CSI 3 as sandy, a comparison between simulations for the two sites (Figure 11a and b), is relevant for verifying the “site equivalence” assumption. The similarity of numerical results at the two stations suggests that dissipation mechanisms (eg. refraction and breaking), do not account for the strong dissimilarity seen in measurements (Figures 11a,b).

5. Conclusions

Previous field experiments have monitored wave evolution along the propagation path, following on the assumption that wave dissipation over muddy bottoms is significant only

for long waves. Here, we compare concurrent wave measurements collected at two WAV-CIS sites, CSI 3 and CSI 5, with the implicit assumption that the two locations are “equivalent”, *i.e.* they would observe the same wave climate if the sedimentary composition on the inner shelf were similar. The “equivalence” of stations CSI 3 and CSI 5 is corroborated by winds and long wave measurements, and supported by the similarity of numerically simulated wave spectra at the two locations. Nearly identical local forcing and offshore wave conditions facilitates the comparative study of mud-induced dissipation in all spectral bands, including high-frequency, short waves.

Numerical simulations suggest that the significant differences in wave conditions at the two locations result from the different sedimentary fabrics of the sea bed, and that wave attenuation in the cohesive sedimentary environment is a leading order effect, observable across the spectrum. Long waves, here defined as having frequencies less than 0.2 Hz, are attenuated at the muddy site compared to the sandy site by an order of magnitude in variance. The effect is consistent with bottom friction, and has been observed previously, although no comparison with sandy environments has been reported.

The experimental setting used here allows for a comparative study of short wave evolution. Observations show that short waves, ($f \geq 0.2$ Hz) are also strongly attenuated. Short waves have comparable energy levels during periods of high winds (strong forcing), but decay much faster and to lower levels at the muddy site, as soon as the wind forcing ceases. Strong evidence of sediment re-working by storms, as well as their weak interaction with the bottom, suggest their damping is likely due to processes related to sediment resuspension or increased thickness of a fluid-mud layer.

Mud-induced short wave dissipation is not understood, and is the object of continuing research. No systematic measurements of the sediment state (eg. spatial distribution of concentration, density) were available at the time of this study, and therefore, no attempt was made here to correlate quantitatively sediment characteristics and sea states. Observations suggest that short time scales of the geological response to hydrodynamic forcing induce a strong coupling of waves, currents and sediment transport processes. Changes in the physical properties of the water column induced by suspended sediments have strong, spectrum-wide effects on surface waves, which eventually feed back into current evolution and sediment deposition and accretion. Understanding this complex of processes could require simultaneous high resolution measurement of multiple variables, such as wave spectral density, spatial distribution of velocities, and sediment concentration.

Numerical simulations carried out using a third-generation spectral wave model underscores the extent to which wave processes in cohesive sedimentary environments differ from the better studied sandy sea beds. Simulations overpredict wave energy at the muddy site by a wide margin. The importance of short wave dissipation and the limitations of the “long wave paradigm” are apparent also at the level of numerical implementations. Simple numerical experiments to increase wave dissipation by manipulating existing bottom friction parametrizations result in increasingly damped low frequency waves, with almost no effects in the high frequency part of the spectrum.

Efforts are under way at CSI to deploy additional WAVCIS stations on the shelf, as well as to complement WAVCIS stations with turbidity sensors (optical backscatter sensors, salinity sensors etc). Sediment concentration data will be used in conjunction with wave and vertical current distribution, to investigate the evolution of mud stratification

under a wide variety of sea conditions. New approaches to mathematical and numerical modelling of wave propagation in heterogeneous sedimentary environments, which take into account the strong coupling between hydrodynamics and mud rheology evolution, are under development.

Acknowledgments. This research was supported by the Office of Naval Research, award No. N00014-03-1-0200, and the Louisiana Board of Regents, contract LEQSF(2002-5)-RD-A-10.

WAVCIS program is supported by funding from NOAA, contract No. NA160C-2938, FEMA, contract No. 2529-01-01, LDNR, contract No. 2503-00-21, and OSRADP, contract No. 169-70-4150. The authors are grateful to ChevronTexaco for logistical and infrastructure support. The CSI Field Support Group provided excellent logistical support.

References

- Allison, M. A., G. C. Kineke, E. B. Gordon, and M. A. Goñi, Development and reworking of a seasonal flood deposit on the inner continental shelf off the Atchafalaya River. *Continental Shelf Res.* 20, 2267-2294, 2000.
- Booij, N., R.C. Ris, and L.H. Holthuijsen, A third generation wave model for coastal regions: Part I: model description and validation, *J. Geophys. Res.*, V104, 7649-7666, 1999.
- Chou, H.-T., Rheological response of cohesive sediments to water waves, *Ph. D. Thesis*, Civ. Eng., UC. Berkeley, 1989.

- Chou, H.-T., M.A. Foda, and J.R. Hunt, Rheological response of cohesive sediments to oscillatory forcing, In: *Nearshore and Estuarine Cohesive Sediment transport, Coastal Estuarine Sci.*, 42, A.J. Mehta ed., 126-148, AGU, Washington DC, 1993.
- Earle M. D., D. McGehee, M. Tubman, Field wave gaging program, wave data analysis standard, *US Army Corps of Engineers, Instr. Rep. CERC-95-1*.
- Foda, A.M., J.R. Hunt, and H.-T. Chou, A nonlinear model for the fluidization of marine mud by waves, *J. Geophys. Res.* 98(C4), 7039-7047, 1993.
- Forristall, G.Z., and A.M. Reece, Measurements of wave attenuation due to a soft bottom: the SWAMP experiment, *J. Geophys. Res.*, 90(C2), 3367-3380, 1985
- Gade, H.G. Effects of a non-rigid impermeable bottom on plane surface waves in shallow water, *Ph. D. Thesis*, Texas A&M University, 35 pp, 1957.
- Hodur, R. M., 1993: Development and Testing of the Coupled Ocean/Atmosphere Mesoscale Prediction System (COAMPS). NRL/MR/7533-93-7213. Naval Research Laboratory, 81 pp.
- Jiang, F., and A.J. Mehta, Mudbanks of the Southwest Coast of India IV: Mud viscoelastic properties, *J. Coastal Res.* 11/33, 918-926, 1995.
- Lee, S.-C., Response of mud shore profiles to waves. *Ph.D. Thesis*, University of Florida, Gainesville.
- Li, Y., and A.J. Mehta, Fluid mud in wave dominated environment revisited, In: *Coastal and Estuarine Fine Sediment Processes, Proc. Mar. Sci.* 3, McAnally, W.H., and A.J. Mehta (eds.), 79-93, 2000.
- Maa, P.-Y., and A.J. Mehta, Soft mud response to water waves, *J. Waterw., Port, Coastal and Ocean Eng.* 116(5), 634-650, 1991.

- Mei, C.C., and K.-F. Liu, A Bingham-plastic model for a muddy sea bed under long waves, *J. Geophys. Res.* *92(C13)*, 14,581-14,594, 1987
- Mossa, J and H. H. Roberts, Synergism of riverine and winter storm-related sediment transport processes in Louisiana's coastal wetlands, *Gulf Coast Assoc. of Geological Soc. Trans.* *40*, 635-642, 1990.
- Murray, S.P. An observational study of the Mississippi -Atchafalaya coastal plume: Final report. *OCS Study MMS 98-0040*, US Dept. of Interior. Minerals Mgmt. Service, Gulf of Mexico OCS Region, New Orleans, LA. 513 pp, 1997.
- Penland S., R. Boyd, and J. R. Suter, Transgressive depositional systems of the Mississippi Delta Plain: a model for barrier shoreline and shelf sand development, *J. Sedimentary Petrology* *58(6)*, 932-949, 1988
- Pepper, D. A. and G. W. Stone, Atmospheric forcing of fine-sand transport on a low energy inner shelf: south-central Louisiana, USA *Geo-Mar. Lett.* *22*, 33-41, 2002
- Roberts, H. H., O.K. Huh, S. A. Hsu, L. J. Rouse, and D. A. Rickman, Winter storm impacts on the chenier plain coast of Southwestern Louisiana, *Gulf Coast Assoc. of Geological Soc. Trans.* *39*, 515-522, 1989
- Rogers, E, P. Hwang, and D. Wang, Investigation of wave growth and decay in the SWAN model: three regional scale applications. *J. Phys. Oceanogr.*, *in print*.
- Sterling, G.H., and E.E Strohbeck, The failure of the South Pass 70"B" platform in Hurricane Camille. *Fifth Offshore Technology Conf.*, Houston, Texas, preprint 1898, 1973.
- Stone, G. W., A. Sheremet, X. Zhang, Q. He, B. Liu, and B. Strong, Landfall of two tropical systems seven days apart along Southcentral Louisiana, USA, *Proc. Coastal*

Sediments '03, Clearwater Beach, Florida, p. 333-334.

Tubman, M.W., and J.N. Suhayda, Wave action and bottom movements in fine sediments

Proc. 15-th Coastal Eng. Conf., Honolulu, Hawaii, 1976.

Walker, N. D. and A. B. Hammack, Impacts of winter storms on circulation and sediment

transport: Atchafalaya-Vermilion Bay region, Louisiana, USA, *Proc. 15-th J. Coastal*

Res. 16(4), 996-1010, 2000.

Wells, J. T. and G. P. Kemp, Atchafalaya mud stream and recent mudflat progradation:

Louisiana chenier plain. *Gulf Coast Assoc. of Geological Soc. Trans. 31*, 409-416, 1981.

Wright, L. D., C. R. Sherwood, and R. W. Sternberg, Field measurements of fairweather

bottom boundary layer processes and sediment suspension on the Louisiana inner con-

tinental shelf, *Mar. Geol. 140*, 329-245, 1997.

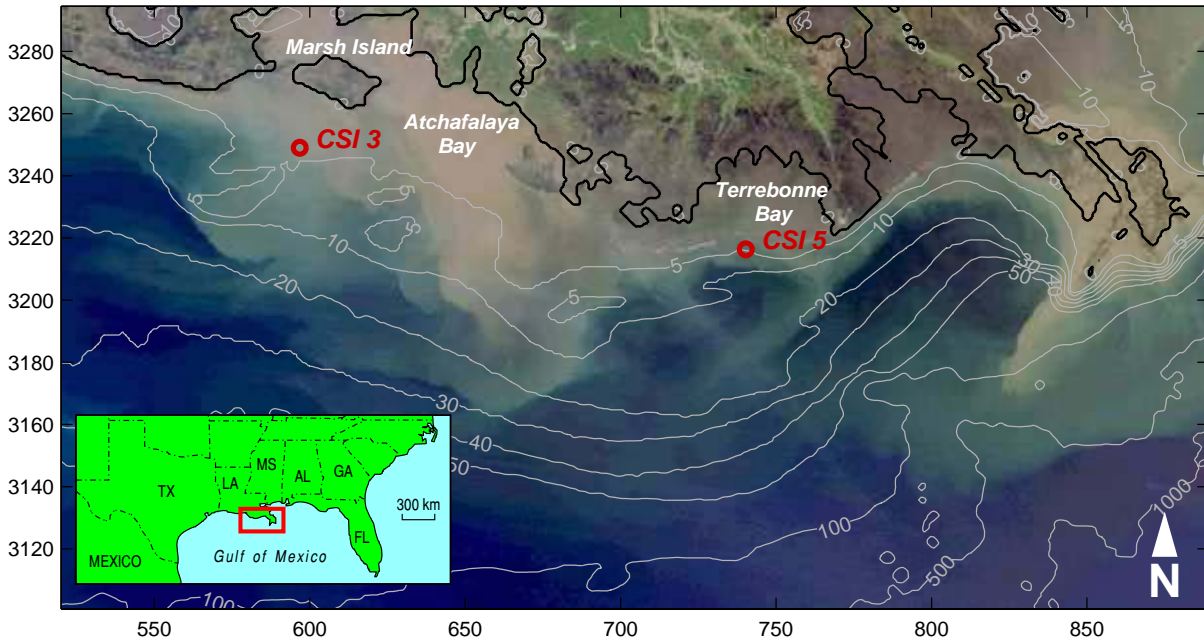


Figure 1. True-color TERRA-1 Modis satellite image of the Louisiana coast at 250 m resolution (Earth Scan Laboratory, www.esl.lsu.edu), overlaid with bathymetry contours at 1-km resolution. Contours are given in meters. Coordinates are given in kilometers with respect to UTM 1983, Zone 15. Some features visible in the image, such as the barrier islands, are not resolved at the 1-km resolution of the bathymetric grid. WAVCIS stations CSI 3 and CSI 5 are marked by circles. The light brown tint is correlated to high surface sediment concentrations. Inset: Northern Gulf of Mexico, with the area shown in the satellite image marked in red.

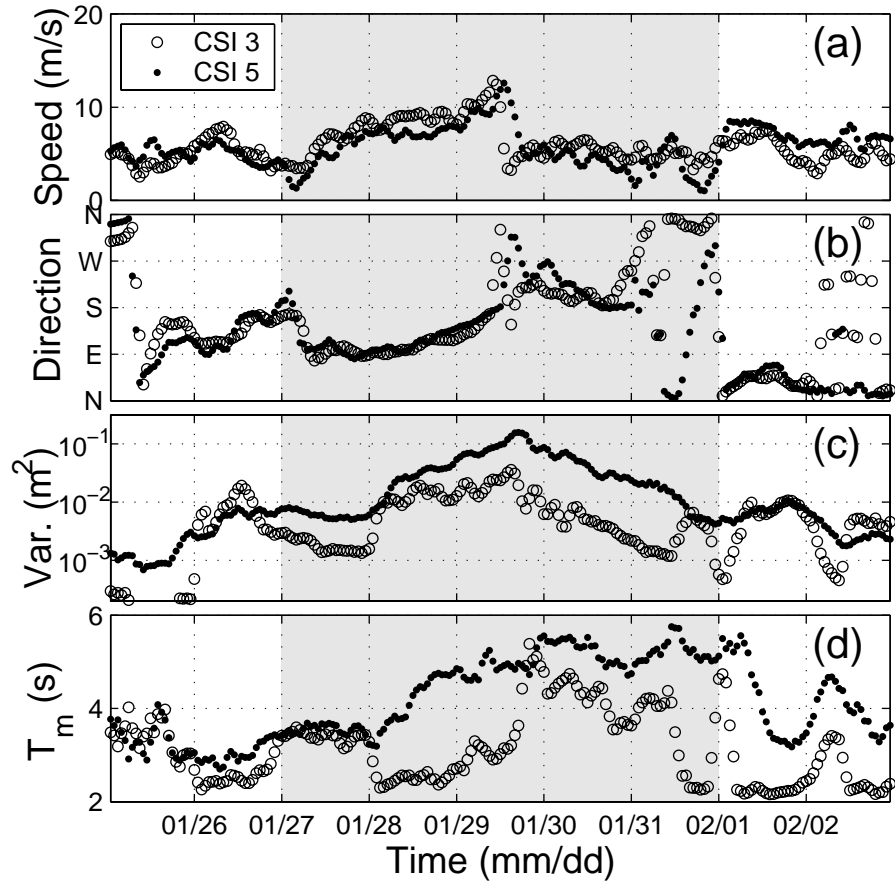


Figure 2. Wind and waves observations at CSI 3 and CSI 5 versus time. a) Sustained wind speed at the 10 m elevation. b) Wind direction. c) Wave variance. d) Mean period.

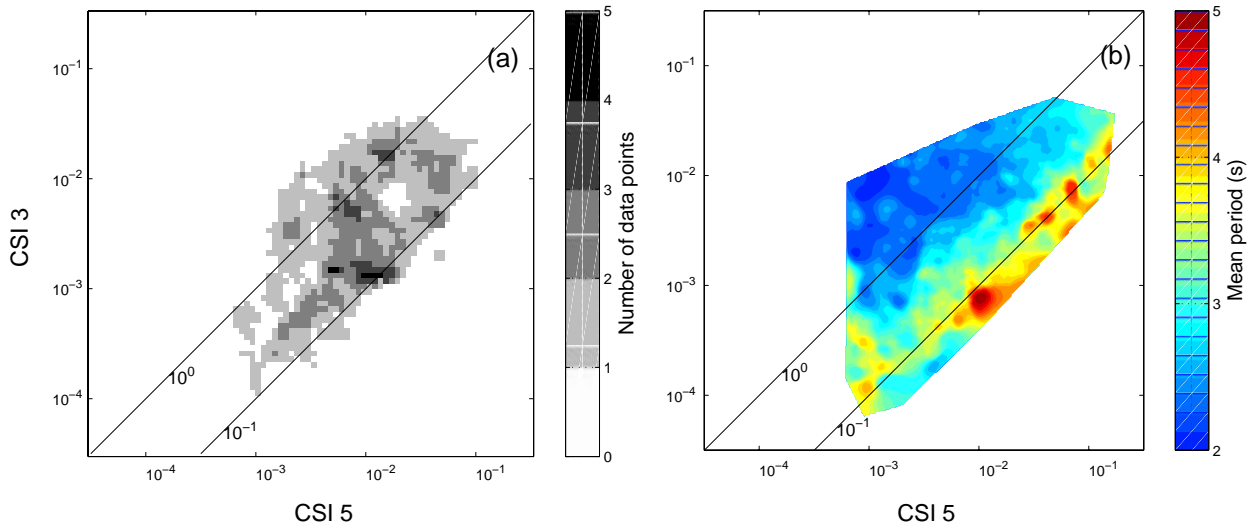


Figure 3. Observed CSI 3 and CSI 5 variance and mean period, for the entire 4-month time series. a) Data point distribution (each point represents an hourly 16-min measurement) versus variance levels at the two observation stations (the variance is in m^2). The distribution was resampled in a rectangular grid. Gray levels represent the number of data points in a bin. b) Distribution (reasmped) of mean periods. Values are bin-averages. Lines corresponding to ratios 1 and 0.1 are plotted for reference.

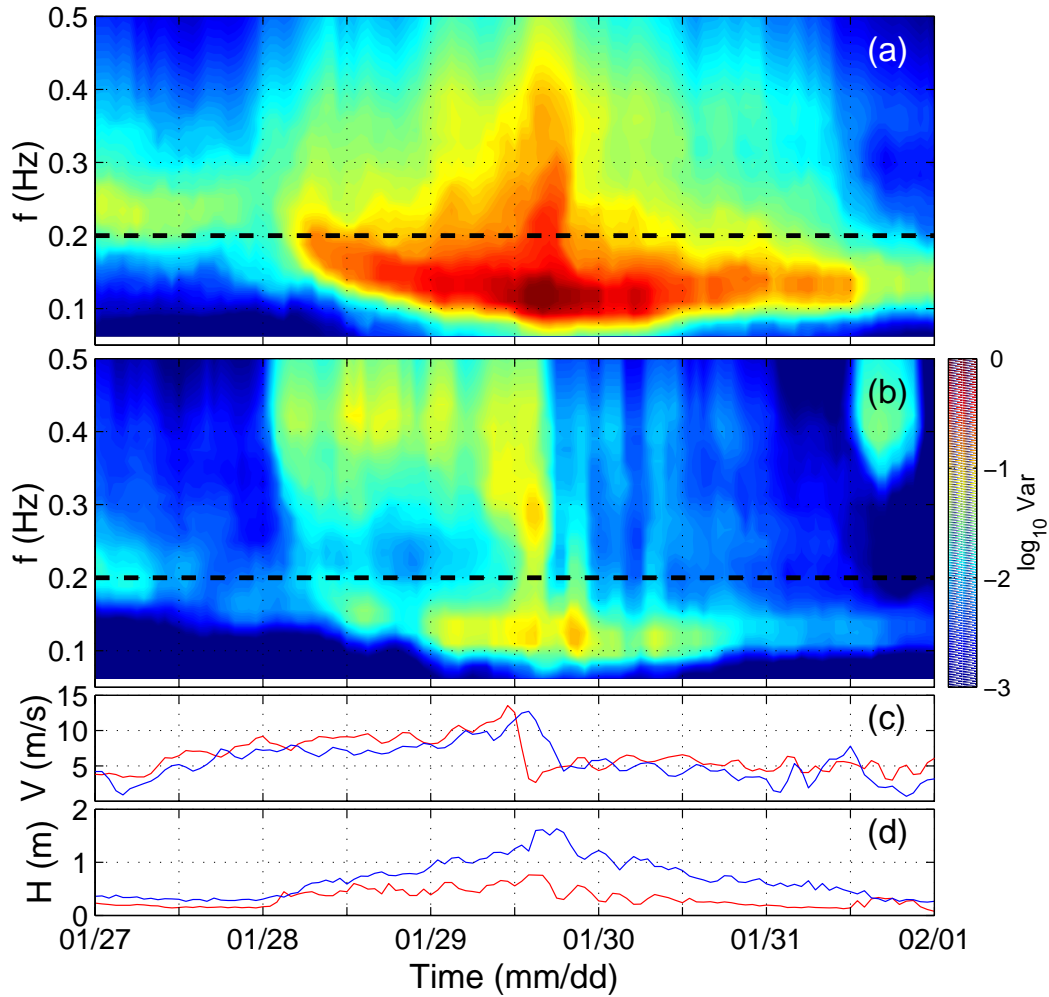


Figure 4. Spectral evolution during the storm of Feb. 22-28 (grayed area in Figure 2). a) and b) Contours of spectral evolution at CSI 5 and CSI 3, respectively. Dashed line at $f = 0.2$ Hz separates low and high frequency bands discussed in the text and used in Figures 5 and 7. The boundary value of 0.2 Hz is arbitrary, but seems to agree with the structure of the spectra. c) Wind speed. d) Significant wave height (red – CSI 3, blue – CSI 5).

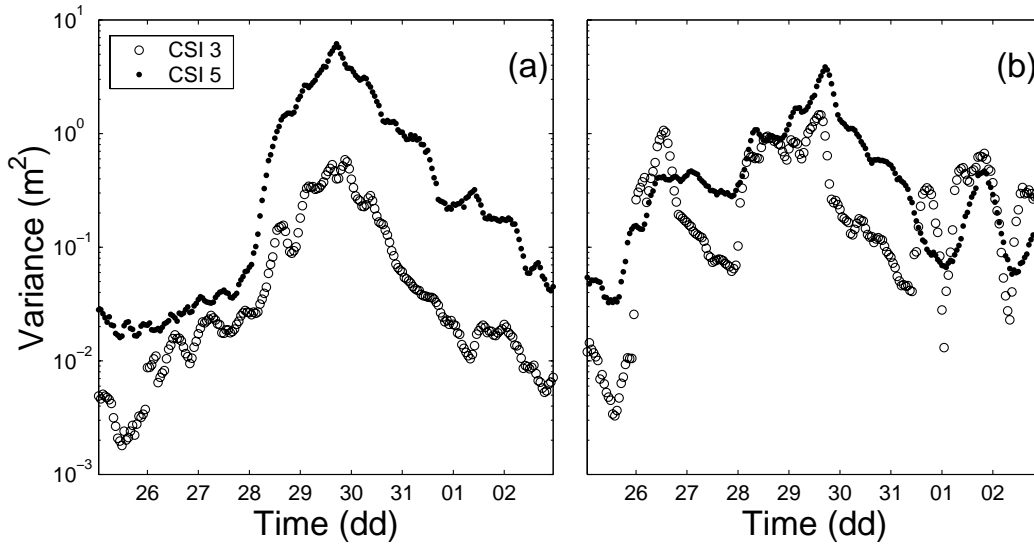


Figure 5. Band-integrated variance versus time, storm of Feb. 22-28 (grayed area in Figure 2). a) Low frequency band ($f < 0.2$ Hz). b) High frequency band ($f \geq 0.2$ Hz, see also Figure 4).

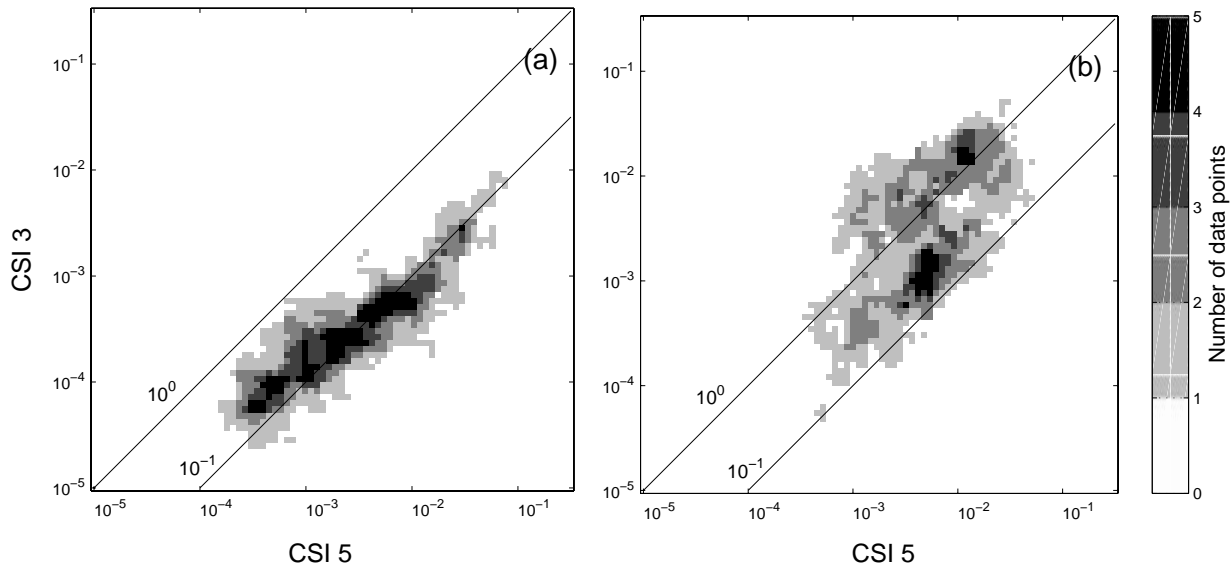


Figure 6. Comparison of long and short wave variance (m^2) levels measured at CSI 3 and CSI 5, for the entire 4-month period studied (same format as Figure 3a). a) Low frequency band ($f < 0.2$ Hz). b) High frequency band ($f > 0.2$ Hz, see also Figure 4).

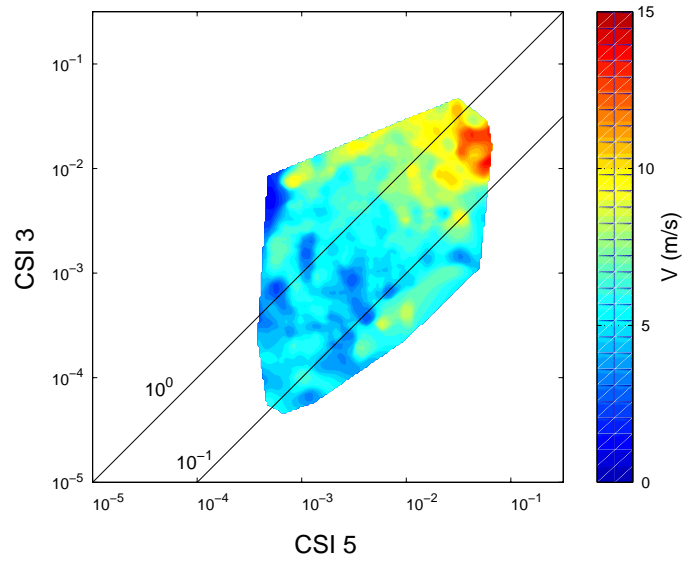


Figure 7. Distribution of sustained wind speed (V) as a function of high frequency band variance (m^2) values at CSI 3 and CSI 5 (compare with Figure 6b).

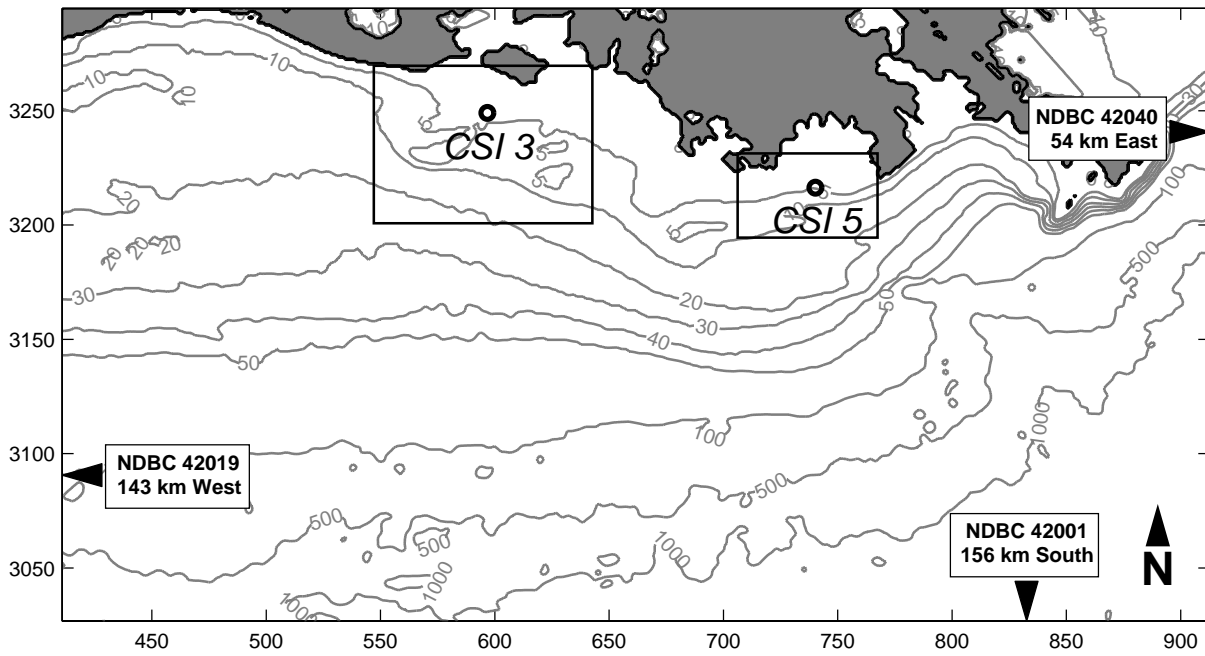


Figure 8. Coarse resolution computational grid, with nested grids for CSI 3 and CSI 5 (red rectangles). The positions of NDBC buoys 42019, 42001 and 42040 relative to the edge of the coarse grid are indicated by arrows. Depth contours are in meters, coordinates in kilometers with respect to UTM 1983, Zone 15.

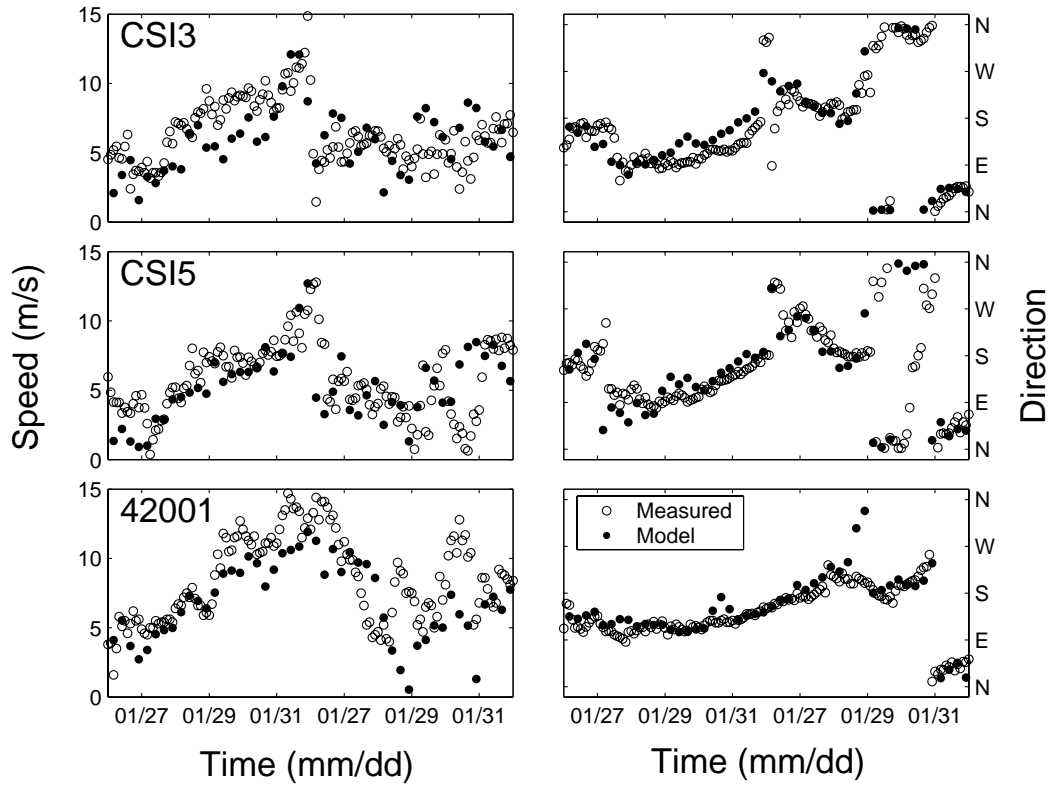


Figure 9. Wind speed and direction versus time, during the 27 Jan. - 01 Feb. 2001 storm. a), c), and d) Wind speed at stations CSI 3, CSI 5, and NDBC Buoy 42001, respectively. b), d), and f) Wind direction. Model wind values were interpolated from COAMPS surface wind field output at approximately 22 km resolution.

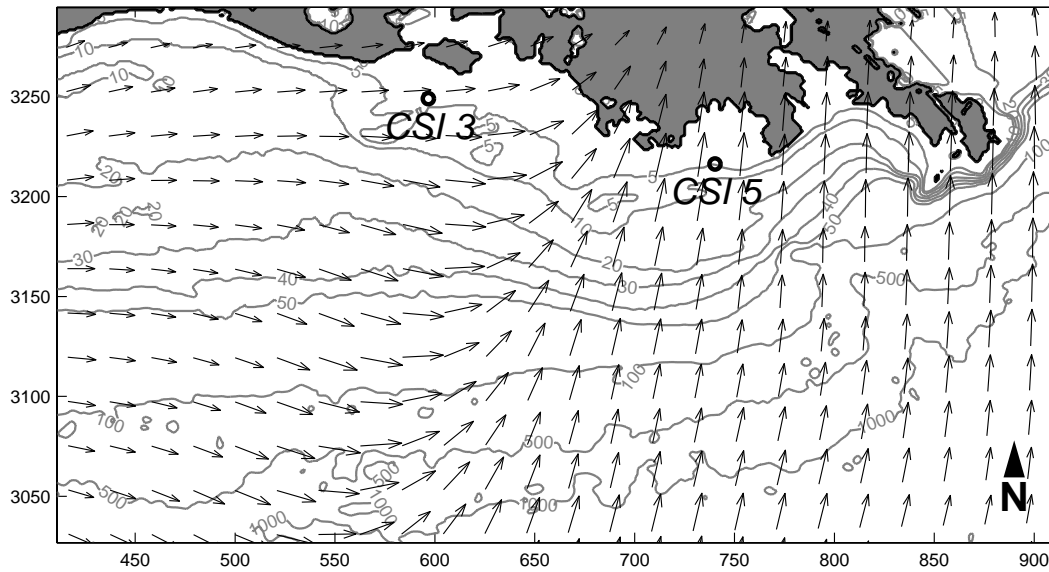


Figure 10. COAMPS surface wind field for the area covered by the coarse computational grid, 29 Jan. 2001, 2100 LST. Arrows are proportional to wind speed. Maximum wind speed shown in this plot is 13.0 m/s. The cold front is indicated by a rotation of wind direction along a line passing approximately SW to NE, between CSI 3 and CSI 5.

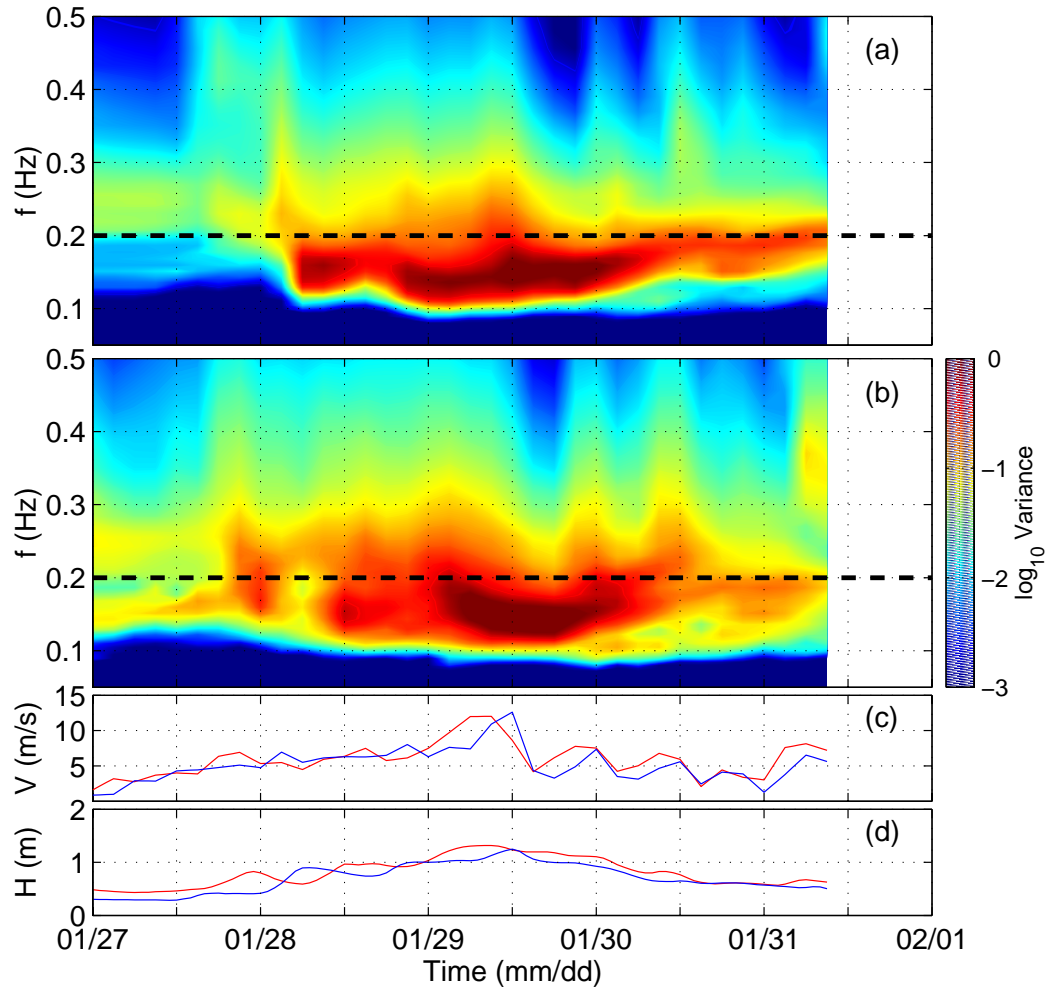


Figure 11. Numerical simulations: Spectral evolution, 27 Jan. to 01 Feb. 2001 storm. a, b) Contours of the spectral evolution, c) wind speed and d) significant wave height vs. time (red: CSI 3, blue: CSI 5).